ADVANCED OPTICAL MATERIALS
www.advopticalmat.de

Nonlinear Current Injection in Hexagonal Boron Nitride using Linearly Polarized Light in a Deeply Off-Resonant Regime

Wenwen Mao, Angel Rubio,* and Shunsuke A. Sato**

Light-induced electron dynamics in monolayer hexagonal boron nitride is theoretically investigated under the influence of two-color linearly-polarized laser fields at frequencies ω and 2ω, by solving the time-dependent Schrödinger equation with a tight-binding model. In the weak field regime, it is confirm that the injection of ballistic current arises from the breakdown of time-reversal symmetry. This phenomenon is attributed to quantum interference between two distinct excitation paths: a one-photon ($2\hbar\omega$) absorption path and a two-photon ($\hbar\omega$) absorption path. In a strong field regime, the analysis reveals that the two-color laser fields may generate a substantial population imbalance within momentum space, consequently facilitating the injection of ballistic current even in a deeply off-resonant regime. The findings demonstrate that a pronounced population imbalance exceeding 30% of excited electrons can be realized without relying on the ellipticity of the fields. This highlights the potential of linearly polarized light for efficient photovoltaic effects and valley population control in 2D systems and heterostructures.

1. Introduction

The photovoltaic effect involves the conversion of light into a flow of charges, forming a fundamental phenomena for clean energy generation in our society. Consequently, extensive investigations into the photovoltaic effect have been conducted from various perspectives, involving both fundamental and technological points of view. Among the various mechanisms of the photovoltaic effects, the shift-current, classified as a second-order nonlinear optical effect,[1] has been attracting substantial attention for its potential in achieving a very efficient light-to-current conversion.[2–5]

Another noteworthy second-order nonlinear optical effect is the injection current,[1,6,7] which can be induced by the breaking of time-reversal symmetry through elliptically or circularly polarized light, in addition to the breaking of intrinsic spatial inversion symmetry. While the shift-current occurs solely during laser irradiation, the injection current may persist even after the laser irradiation ends. The persistence time of the injection current is only limited by decoherence and dissipation effects that disturb the phenomenon after the irradiation is turned off. This persistent current arises from the population imbalance in the Brillouin zone caused by the laser excitation.[1]

Expanding beyond the second-order nonlinear effect, the photovoltaic effects with an intense few-cycle laser pulse have been explored.[8–13] Such a laser pulse can extrinsically break spatial inversion symmetry. Moreover, a strong field can introduce a highly nonlinear excitation channel, such as the tunneling excitation path. Through the combination of extrinsic spatial inversion symmetry breaking and intense nonlinear interactions between light and matter, an intense few-cycle laser pulse may induce a direct current (dc-current) even in a material with intrinsic inversion symmetry. Because the photovoltaic effect with a few-cycle pulse depends on breaking the inversion symmetry of the light fields, the induced current can be manipulated by controlling the intensity and carrier envelope phase of the pulse.[8,11]

In recent research, an effective method for controlling valley population has emerged, involving the combination of two circularly polarized lights with different frequencies, denoted as ω and 2ω, specifically studied in the context of 2D systems.[14,15] Each circularly polarized light individually breaks time-reversal symmetry, and when combined, the fields can additionally break spatial inversion symmetry. This dual breakdown of time-reversal and spatial inversion symmetries leads to the creation of a

W. Mao, A. Rubio, S. A. Sato
Max Planck Institute for the Structure and Dynamics of Matter
Luruper Chaussee 149, 22761 Hamburg, Germany
E-mail: wenwen.mao@mpsd.mpg.de; angel.rubio@mpsd.mpg.de; ssato@ccs.tsukuba.ac.jp
A. Rubio
Center for Computational Quantum Physics (CCQ)
Flatiron Institute
162 Fifth Avenue, New York, NY 10010, USA
S. A. Sato
Center for Computational Sciences
University of Tsukuba
Tsukuba 305-8577, Japan

The ORCID identification number(s) for the author(s) of this article can be found under https://doi.org/10.1002/adom.202400651

DOI: 10.1002/adom.202400651

population imbalance in momentum space following laser excitation, resulting in a persistent net charge flow even after the laser irradiation ends. Notably, this methodology has been extended to numerical studies with first-principles calculations applied to bulk solids.[16]

Addressing the photovoltaic effect within the perturbative regime, significant attention has been directed toward the description of the injection of dc current using two-color linearly polarized light.[17–23] The early investigation has particularly emphasized the interplay between a fundamental frequency, denoted as ω, and its second harmonic, 2ω.[17–19] The utilization of two-color fields, such as ω and 2ω, has opened a potential to break the time-reversal symmetry of the systems, even when the combined field is linearly polarized. This symmetry breaking leads to a population imbalance induced by laser irradiation, consequently resulting in dc-current injection. The population imbalance in this scheme is caused by quantum interference between two excitation paths: One is the two-photon absorption process with photons at the frequency ω, while the other is the one-photon absorption process with photons at the frequency 2ω. Hence, this protocol for dc-current injection is known as quantum interference control (QuIC).[24] By manipulating the relative phase of the optical fields at frequencies ω and 2ω, QuIC can be applied to achieve control over one- and two-photon absorption processes, often referred to as (1 + 2 QuIC). Subsequently, the scope of QuIC has been broadened to involve general integer combinations, denoted as (M + N QuIC).[21,23] In this extended scheme, two-color laser fields operating at frequencies ω and ω' induce M- and N-photon absorption processes, respectively.

Despite the considerable interest in the nonlinear photovoltaic effect, there has been limited exploration of efficient current injection in the deeply off-resonant regime with multi-cycle light pulses, especially using linearly polarized light. In a previous study,[14] deeply off-resonant bi-circular laser fields with frequencies ω and 2ω were utilized to create a substantial population imbalance in the Brillouin zone. However, in principle, the use of linearly polarized light with two frequencies is sufficient to break time-reversal symmetry. Therefore, efficient injection of dc-current and the creation of a substantial population imbalance can be realized by employing two-color linearly polarized laser fields with frequencies ω and 2ω, without relying on the ellipticity of light. Furthermore, such analysis with linearly polarized light will fill a gap between a novel nonlinear optical phenomenon with bi-circularly polarized light in the highly nonlinear regime and the traditional QuIC in the perturbative regime, providing novel insights into nonlinear optical phenomena.

In this study, we theoretically investigate dc-current injection and the generation of population imbalance through the application of two-color linearly polarized laser fields with frequencies ω and 2ω. For practical analysis, we examine the light-induced electron dynamics in a prototypical 2D material, monolayer hexagonal boron-nitride (h-BN), using a simple tight-binding approximation. In the quantum dynamics simulation, we find that ballistic current can be induced even in the deeply off-resonant regime with two-color linearly polarized light. Furthermore, we demonstrate that a significant population imbalance is formed even without relying on the ellipticity of light. These findings may pave the way for ultrafast and efficient control of electron population in matter using multi-color linearly polarized light.

2. Theoretical Methods

In this section, we provide a brief explanation of the theoretical methods used to investigate light-induced electron dynamics and evaluate the light-induced current in monolayer h-BN. To describe the electronic structure of h-BN, we employ the following tight-binding Hamiltonian:

$$\hat{H}(\mathbf{k}) = \begin{pmatrix} \epsilon_B & t_0 f(\mathbf{k}) \\ t_0 f(\mathbf{k})^* & \epsilon_N \end{pmatrix} \tag{1}$$

where ϵ_B and ϵ_N represent the on-site energies for boron and nitrogen sites, respectively. The nearest neighbor hopping is denoted by t_0, and the phase factor, $f(\boldsymbol{k})$, is defined as $f(\boldsymbol{k}) = e^{i\boldsymbol{k}\cdot\boldsymbol{\delta}_1} + e^{i\boldsymbol{k}\cdot\boldsymbol{\delta}_2} + e^{i\boldsymbol{k}\cdot\boldsymbol{\delta}_3}$ with the nearest-neighbor vectors $\boldsymbol{\delta}_j$.[25] In this work, we set $\epsilon_B - \epsilon_N$ to 5.9 eV to reproduce the bandgap of h-BN, which is about 5.9 eV computed with first-principles calculations.[26] The nearest neighbor hopping, t_0, is chosen as 2.64 eV, in accordance with previous work.[25] The lattice constant is set to 2.5 Å. The resulting electronic structure yields bandgap minima of $\epsilon_B - \epsilon_N = 5.9$ eV at K and K' points in the Brillouin zone.

To describe light-induced electron dynamics, we employ the following time-dependent Schrödinger equation for each k-point:

$$i\hbar\frac{d}{dt}|\psi_k(t)\rangle = \hat{H}\left(\boldsymbol{k} + \frac{e\boldsymbol{A}(t)}{\hbar}\right)|\psi_k(t)\rangle \tag{2}$$

where $\boldsymbol{k}$ is the Bloch wavevector, and $|\psi_k(t)\rangle$ represents the single-particle electronic wavefunction at $\boldsymbol{k}$. The vector potential $\boldsymbol{A}(t)$ is related to the applied electric field $\boldsymbol{E}(t)$ through $\boldsymbol{E}(t) = -d\boldsymbol{A}(t)/dt$. In the Hamiltonian, the wavevector shifts $\boldsymbol{k} \to \boldsymbol{k} + e\boldsymbol{A}(t)/\hbar$ is introduced by using the Peierls substitution.[27]

By employing the time-dependent wavefunctions, $|\psi_k(t)\rangle$, we evaluate the induced current as

$$J_k(t) = \frac{1}{(2\pi)^2}\int_{BZ} d\boldsymbol{k}\langle\psi_k(t)|\hat{J}_k(t)|\psi_k(t)\rangle \tag{3}$$

here, $\hat{J}_k(t)$ is the current operator and is defined as

$$\hat{J}_k(t) = \frac{\partial}{\partial\boldsymbol{k}}\hat{H}\left(\boldsymbol{k} + \frac{e\boldsymbol{A}(t)}{\hbar}\right) \tag{4}$$

Note that this current operator is widely used, and it can also describe phenomena related to Berry curvature, such as anomalous Hall effects.[28,29]

For practical simulations, we employ the following expression for the vector potential of the applied two-color fields:

$$\boldsymbol{A}(t) = -\boldsymbol{e}_p\frac{E_0}{\omega}\left[\cos(\omega t + \theta) + \frac{1}{4}\cos(2\omega t + \phi + 2\theta)\right] \times \cos^4\left(\frac{\pi}{\tau}t\right) \tag{5}$$

within the interval $-\tau/2 < t < \tau/2$ and zero outside this range. Here, $\boldsymbol{e}_p$ represents a unit vector along the polarization direction of the laser field, E_0 denotes the peak field strength, ω is the fundamental frequency, and τ is the duration of the laser field pulse. We introduce a relative phase ϕ between the two-color fields and

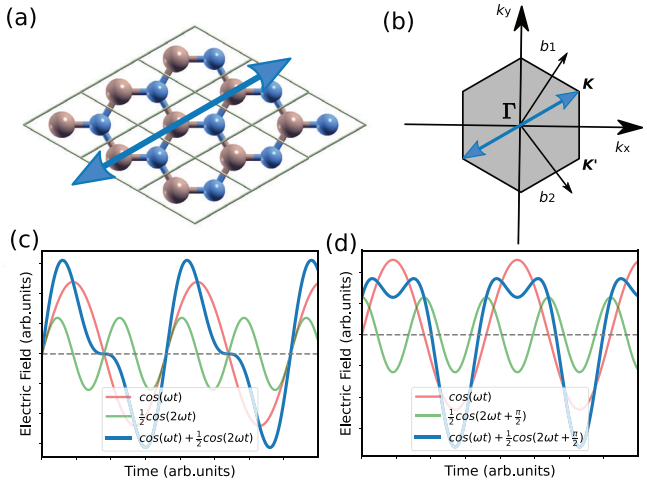

Figure 1. a) Atomic configuration of monolayer *h*-BN and b) the Brillouin zone are shown. In each panel, the blue arrow shows the laser polarization direction. The time profiles of the electric field given by Equation (5) are shown for (c) $\phi = 0$ and (d) $\phi = \pi/2$.

a global phase θ as a common phase for the two fields. The relative phase governs quantum interferences among different excitation paths induced via ω and 2ω laser fields, while the global phase is utilized to extract a dc-like response from the quantum dynamics simulations.

3. Results

3.1. Third-Order Nonlinear Regime: 1 + 2 QuIC

In this section, we revisit the 1 + 2 QuIC process, which is a third-order nonlinear optical process for injecting a dc current using two-color fields, by employing the methods introduced in Section 2. For practical calculations, we set the laser polarization direction, $\boldsymbol{e}_p$, with the Γ–*K* direction, as illustrated in **Figure 1**a,b. Furthermore, the pulse duration, τ, is set to 40 fs.

By utilizing two-color fields with frequencies ω and 2ω, it is possible to induce a population imbalance and, consequently, a dc current by extrinsically breaking the time-reversal symmetry. This can be achieved by manipulating the relative phase ϕ in the vector potential described in Equation (5). Figure 1 c illustrates the electric field generated by the vector potential with a relative phase of $\phi = 0$, while Figure 1 d presents the field with a relative phase of $\phi = \pi/2$. It is evident that the field with $\phi = 0$ in Figure 1c breaks the time-reversal symmetry, as $\boldsymbol{E}(t) \neq \boldsymbol{E}(-t)$, while the field with $\phi = \pi/2$ in Figure 1d maintains the symmetry $\boldsymbol{E}(t) = \boldsymbol{E}(-t)$. Hence, the time-reversal symmetry of the Hamiltonian is broken when $\phi = 0$ and preserved when $\phi = \pi/2$. Consequently, a population imbalance and resulting dc current injection are expected when $\phi = 0$, while symmetric excitation population and the absence of net residual current are anticipated when $\phi = \pi/2$.

For a practical analysis of the dc component of the current induced by the fields, we introduce the global phase θ into the fields of Equation (5), as done in our previous work.[30] Formally, the electric current $\boldsymbol{J}(t)$, evaluated with Equation (3), is a functional of the vector potential $\boldsymbol{A}(t)$. The current becomes a function of the global phase θ when the vector potential follows Equation (5). Hence, we explicitly denote the current as $\boldsymbol{J}(t, \theta)$. By fixing all the laser parameters in Equation (5) except the global phase θ, the dc-like component of the induced current can be extracted through the following integral:

$$J_{\mathrm{dc}}(t) = \frac{1}{2\pi}\int_0^{2\pi} d\theta\, \boldsymbol{J}(t,\theta) \tag{6}$$

here, the higher-frequency components are averaged out, allowing for the clean extraction of the dc-like slow-frequency component.

To illustrate dc current injection, we simulate electron dynamics using the vector potential from Equation (5) with ω set to 3 eV. Note that the photon energy satisfies the condition ($\omega \leqslant E_g \leqslant 2\hbar\omega$) for the 1+2 QuIC process.[18]

Figure 2a shows the calculated dc component of the scaled current, $J_{\mathrm{dc}}(t)/E_0^3$, computed with a relative phase of $\phi = 0$. Results for various field strengths, E_0, are presented. The residual dc current persists even after the laser fields end ($t > \tau/2$). Since the scaled quantity, $J_{\mathrm{dc}}(t)/E_0^3$, remains identical to each other across different field strengths, the dc component of the induced current can be interpreted as a third-order nonlinear optical effect. This observation is consistent with the nature of the 1+2 QuIC process, involving interference between one- and two-photon absorption processes, making it a third-order nonlinear optical phenomenon.

Figure 2b shows the dc component of the scaled current, $J_{\mathrm{dc}}(t)/E_0^3$, computed with a relative phase of $\phi = \pi/2$. In contrast to the results with $\phi = 0$ in Figure 2a, the currents in Figure 2b do not exhibit a persistent dc component after the laser irradiation. This result indicates that the applied field with a relative phase of $\phi = \pi/2$ does not break the time-reversal symmetry, and the population imbalance is not induced, resulting in the absence of a persistent current. It is worth noting that, even in the case of $\phi = \pi/2$, the dc component of the current is induced only during the laser irradiation due to yet another third-order nonlinear optical process.

Having observed that the persistent current after the laser irradiation originating from the population imbalance in the Brillouin zone, we proceed to analyze the population distribution of photocarriers induced by the laser fields. To achieve this, we compute the conduction population distribution by projecting onto the eigenstates of the Hamiltonian defined as:

$$\hat{H}_k|\phi_{bk}\rangle = \epsilon_{bk}|\phi_{bk}\rangle \tag{7}$$

where b is a band index, $|\phi_{bk}\rangle$ is an eigenstate, and ϵ_{bk} corresponds to the eigenvalue. As the Hamiltonian is a 2-by-2 matrix in this work, the band index b denotes either a conduction ($b = c$) or valence ($b = v$) state.

Using eigenstates defined with Equation (7), the conduction population distribution n_{ck} after the laser irradiation can be evaluated as:

$$n_{ck} = \left|\langle\phi_{ck}|\psi_k(t_F)\rangle\right|^2 \tag{8}$$

where t_F is a time after the laser field ends ($t_F > \tau/2$). By imposing the normalization of $|\phi_{bk}\rangle$ and $|\psi_k(t)\rangle$, the computed conduction

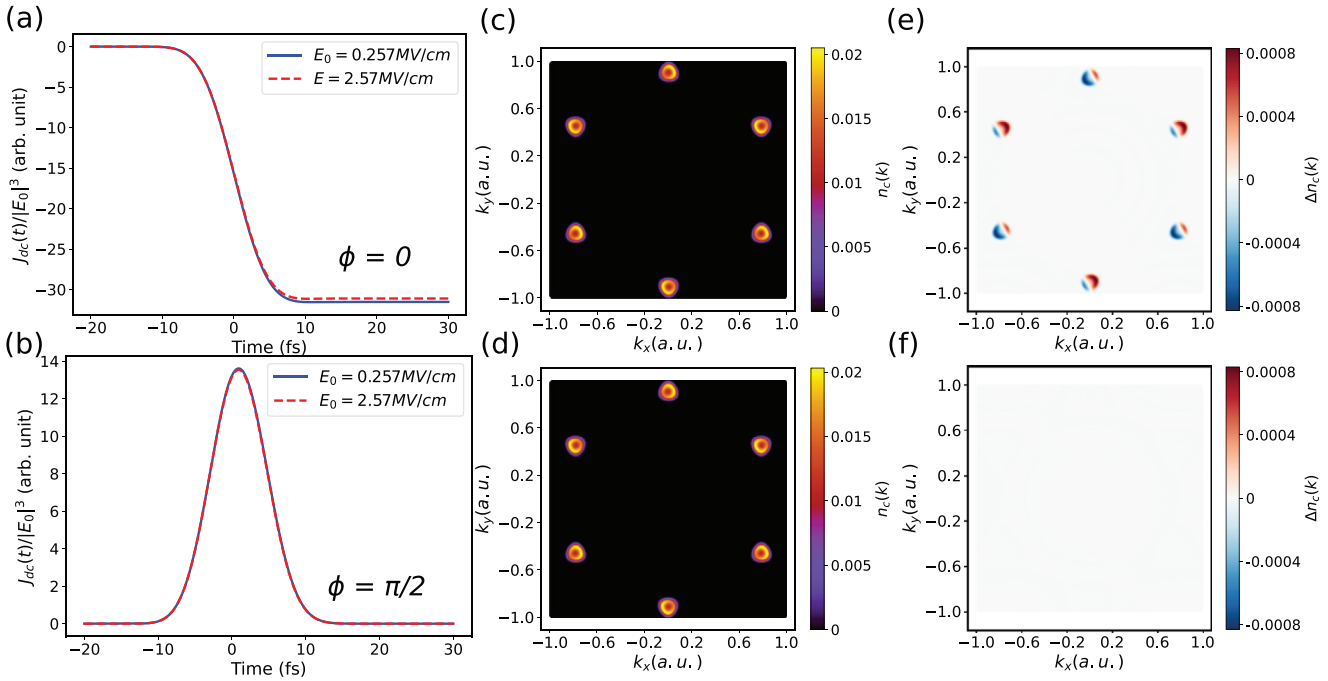

Figure 2. a, b) The dc components of the currents $J_{dc}(t)$ are shown as a function of time. The results using the relative phase of $\phi = 0$ are shown in the panel (a), while those using $\phi = \pi/2$ are shown in (b). c, d) The conduction population distribution $n_c(\boldsymbol{k})$ computed with (c) $\phi = 0$ and (d) $\phi = \pi/2$. e, f) The population imbalance distribution $\Delta n_c(\boldsymbol{k})$ computed with (e) $\phi = 0$ and (f) $\phi = \pi/2$.

population satisfies $0 \leq n_{ck} \leq 1$. It is important to note that, in the present theoretical setup, the conduction population is a constant of motion after laser irradiation since any relaxation processes are not considered.

To assess the persistent dc current after the laser irradiation in Figure 2a, we compute the photo-excited conduction population n_{ck} with a field strength of $E_0 = 2.57$ MVcm^{-1} and a relative phase of $\phi = 0$. The resulting conduction population is shown in Figure 2c. Additionally, Figure 2d shows the conduction population n_{ck} computed using a field with the same strength of $E_0 = 2.57$ MVcm^{-1} but with a different relative phase of $\phi = \pi/2$. In both cases, the conduction populations exhibit pronounced excitations around the K- and K'-points, suggesting that the photo-absorption process is dominated by a one-photon absorption at the photon energy of $2\hbar\omega$ and a two-photon absorption at the photon energy of $\hbar\omega$.

Although the population distributions in Figure 2c,d may initially appear identical, a closer examination reveals distinctions. In the case of the time-reversal symmetry-broken field ($\phi = 0$) in Figure 2c, the population distribution must exhibit an imbalance between time-reversal Kramers pairs (e.g., $\boldsymbol{k}$ and $-\boldsymbol{k}$, or K and K') since there is a persistent current after the laser irradiation, as shown in Figure 2a. In contrast, in the case of the time-reversal field ($\phi = \pi/2$) in Figure 2d, the population distribution n_{ck} should not display such a population imbalance since there is no persistent current.

To illustrate the population imbalance in the Brillouin zone, we define the population imbalance distribution Δn_{ck} as the difference in population between the time-reversal pair k-points, given by $\Delta n_{ck} = n_{ck} - n_{c,-k}$. Since $n_{c,k}$ is bounded by $0 \leq n_{ck} \leq 1$, the population imbalance distribution is bounded by $-1 \leq \Delta n_{ck} \leq 1$. When the external fields preserve time-reversal symmetry, the populations at $\boldsymbol{k}$ and $-\boldsymbol{k}$ are equivalent, resulting in a population imbalance distribution of zero. In contrast, when time-reversal symmetry is broken, non-equivalent populations can be induced at $\boldsymbol{k}$ and $-\boldsymbol{k}$, leading to a finite population imbalance distribution Δn_{ck}.

Figure 2e,f shows the population imbalance distribution, Δn_{ck}, computed from the population distribution presented in Figure 2c,d, respectively. As evident from the figures, when the external field breaks the time-reversal symmetry ($\phi = 0$), a finite population imbalance is induced. In contrast, when the field preserves time-reversal symmetry ($\phi = \pi/2$), the population imbalance vanishes completely.

By manipulating the relative phase ϕ, one can control the magnitude of time-reversal symmetry breaking, allowing for control of the resulting population imbalance and dc current injection.[17] For later convenience, we analyze the persistent dc current by varying the relative phase ϕ. **Figure 3** shows the relative phase ϕ-dependence of the dc current after the laser irradiation, computed using a field with a strength of $E_0 = 2.57$ MVcm^{-1}. The amplitude of the induced dc current is greatest when $\phi = 0$ and $\phi = \pi$, but the signs are opposite for these two phases. Furthermore, the induced dc current continuously changes by manipulating the phase ϕ, reaching zero when $\phi = \pi/2$ and $\phi = 3\pi/2$, where the applied fields recover time-reversal symmetry. This simple phase dependence is consistent with previous works.[17,19]

At the end of this section, we explore the photon-energy dependence of the 1 + 2 QuIC process. This process originates from interference between one- and two-photon absorption processes induced by light with frequencies of ω and 2ω. The fundamental

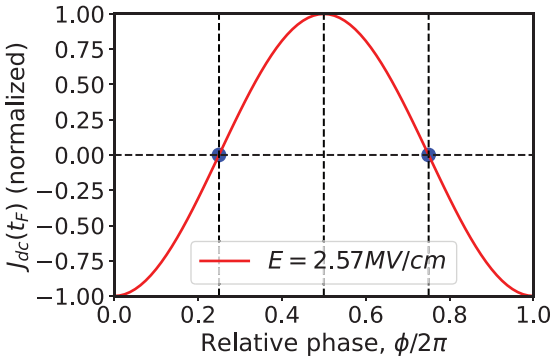

Figure 3. The persistent current $J_{dc}(t_f)$ as a function of the relative phase, ϕ. The results are computed by setting E_0 to 2.57 MVcm^{-1} and $\hbar\omega$ to 3 eV.

photon energy $\hbar\omega$ must satisfy the condition $\hbar\omega \geqslant E_g/2$, where E_g is the band gap. When the fundamental photon energy $\hbar\omega$ is smaller than the gap, both the 1 + 2 QuIC process and the resulting dc current vanish.

To examine this behavior in our theoretical framework, we calculate the dc current after laser irradiation by varying the fundamental frequency ω in Equation (5). **Figure 4a** shows the dc current after the laser irradiation with a field strength of E_0 = 1.03 MVm^{-1}. Consistent with the expected behavior of the

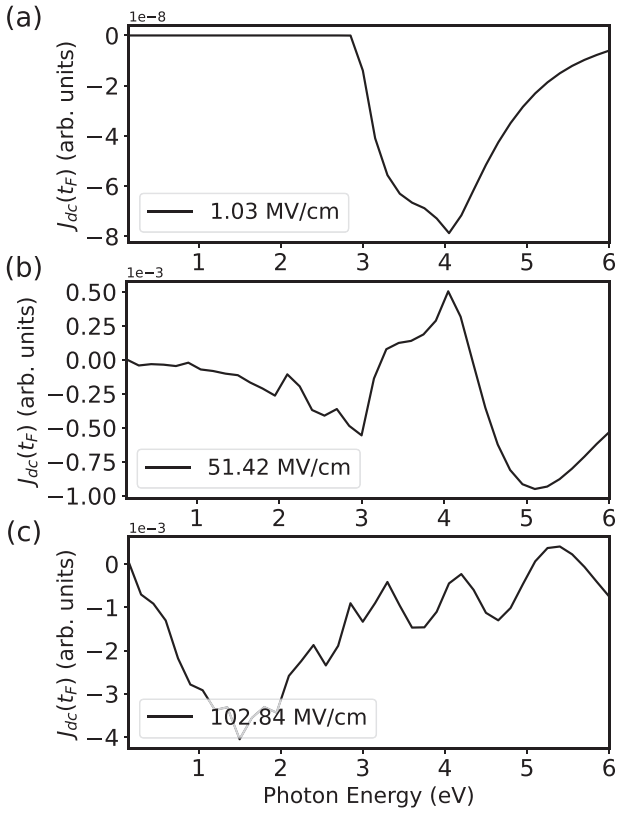

Figure 4. The current after the laser irradiation is shown as a function of the fundamental photon energy $\hbar\omega$. The results computed different field strengths: a) E_0 = 1.03 MVcm^{-1}, b) 51.43 MVcm^{-1}, and c) E_0 = 102.84 MVcm^{-1}.

1 + 2 QuIC process, the residual dc current vanishes when the fundamental photon energy falls below half of the bandgap, $\hbar\omega \leqslant E_g/2$ = 2.95 eV.

To gain insights into this highly nonlinear optical phenomena, we investigate the photon energy dependence of the dc current after laser irradiation while varying the field strength, E_0. Figure 4b,c shows the photon-energy dependence of the persistent current after laser irradiation, computed with a field strength of (b) E_0 = 51.42 MVcm^{-1} and (c) E_0 = 102.84 MVcm^{-1}. Unlike the weak field regime (the 1 + 2 QuIC regime), the dc current can be induced even with deeply off-resonant fields, where the photon energy is smaller than half of the bandgap ($\hbar\omega \leqslant E_g/2$), as evident in Figure 4b. This result suggests that strong laser fields introduce additional paths for exciting electrons involving multiple photons, beyond the two-photon absorption, leading to the creation of population imbalance and a residual dc current even in the deeply off-resonant regime.

As shown in Figure 4c, the magnitude of the dc current after laser irradiation in the deeply off-resonant regime ($\hbar\omega \leqslant E_g/2$) exceeds that in the 1 + 2 QuIC regime ($\hbar\omega \geqslant E_g/2$) when the applied field strength becomes very large. This behavior can be understood by the fact that the ponderomotive energy, $U_p = \frac{e^2E_0^2}{4m\omega_0^2}$, and the corresponding light-induced intraband transitions are larger for lower frequency driving.[31] Consequently, the resulting nonlinear effects and the dc current injection become more significant in the deeply off-resonant regime rather than the resonant condition. In the forthcoming section, we will delve deeper into investigating efficient DC current induction with highly nonlinear optical processes in the deeply off-resonant regime.

3.2. Deeply Off-Resonant Highly-Nonlinear Regime

To explore this mechanism of the dc current injection in the deeply off-resonant regime demonstrated in the previous section, we set the fundamental photon energy $\hbar\omega$ in Equation (5) to 1 eV, a value much smaller than half of the bandgap, $E_g/2$ = 2.95 eV, in this subsection.

We first analyze the light-induced current in the time domain within the deeply off-resonant regime. **Figure 5** shows the dc component of the current, $J_{dc}(t)/E_0^3$, computed with varying field strengths, E_0. Here, the relative phase, ϕ, is set to 0. Clearly, a third-order nonlinear response dominates the induced current when the field strength is weak. Given that the photon energy of the second harmonic is smaller than the bandgap ($2\hbar\omega < E_g$) and the QuIC process is forbidden, the third-order current returns to zero after the laser irradiation. However, as the field strength becomes sufficiently strong, the dc-like component remains finite even after laser irradiation, as shown in Figure 5. This outcome suggests that a higher-order nonlinear process contributes to the ballistic dc current injection beyond the third-order nonlinear effect.

We then examine the dependence of the ballistic current induced by deeply off-resonant light on the relative phase, ϕ. **Figure 6** shows the computed current as a function of the relative phase, ϕ. The calculations were conducted with a field strength of E_0 = 2 × 10 MVcm^{-1}. In alignment with the QuIC case in Figure 3, the persistent current is maximized when the relative phase is ϕ = 0 or ϕ = π, and it vanishes when the applied field

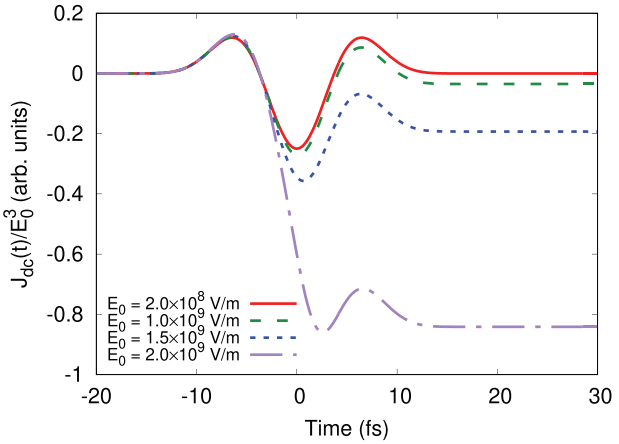

Figure 5. The dc components of the currents, $J_{dc}(t)$, are shown as a function of time. The results are computed with the deeply off-resonant condition, $\hbar\omega = 1.0$ eV.

exhibits time-reversal symmetry ($\phi = \pi/2$ or $\phi = 3\pi/2$). Therefore, even in the deeply off-resonant regime, the direction and magnitude of the persistent current can be controlled by manipulating the relative phase ϕ between the two-color fields at frequencies ω and 2ω.

To elucidate the detailed mechanism of dc current injection with deeply off-resonant light, we analyze how the injected current scales with the field strength E_0. **Figure 7** shows the current amplitude after laser irradiation as a function of the applied field strength. Additionally, a line representing $|E_0|^7$ is included as a reference. As seen from the figure, the induced current is proportional to $|E_0|^7$ in the weak field regime, indicating that the seventh-order nonlinear process dominates the injection of dc current.

The observed scaling law might deviate from the expected scaling of a simple $M + N$ QuIC process, where the M-photon absorption process is induced by light with frequency ω, and the N-photon absorption process is triggered by light with frequency 2ω, resulting in the $(M + N)$-th order nonlinear process. In this context, a six-photon process is required for multi-photon absorption with light of frequency ω, and a three-photon process is anticipated for light of frequency 2ω. Therefore, the expected simple $M + N$ QuIC process corresponds to the ninth-order nonlinear process ($M + N = 6 + 3 = 9$). However, the observed scaling indicates seventh-order nonlinearity. The apparent discrepancy between the observed and expected nonlinearities of the injected dc current can be understood if an additional excitation channel involving a four-photon absorption process, where two photons at frequency ω and the other two photons at frequency 2ω combine to excite electrons, is active. This additional four-photon excitation channel interferes with the three-photon absorption process at the photon energy of $2\hbar\omega$, resulting in seventh-order ($7 = 3 + 4$) nonlinear current injection.

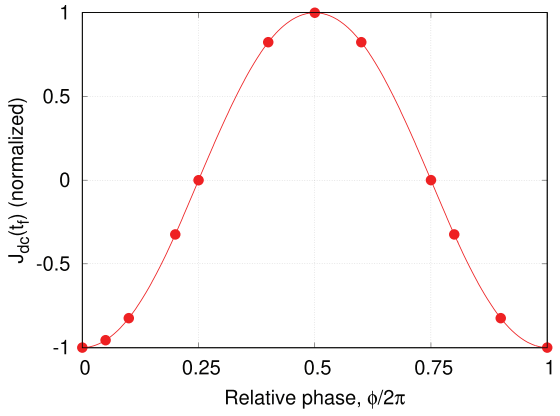

Figure 6. The persistent current, $J_{dc}(t_f)$, is shown as a function of the relative phase ϕ. The results are computed with the deeply off-resonant condition, $\hbar\omega = 1.0$ eV.

To further elucidate the nonlinearity of the light-induced electron dynamics, we computed the number of photo-excited carriers after laser irradiation using

$$N_{ex} = \frac{2}{A_{BZ}} \int_{BZ} d\boldsymbol{k} n_{c,\boldsymbol{k}} \tag{9}$$

where $A_{BZ} = \int_{BZ} d\boldsymbol{k}$, is the area of the Brillouin zone.

Figure 7b shows the number of excited electrons as a function of the field strength, E_0, along with a reference line proportional to $|E_0|^6$. In the weak field regime, the number of excited electrons demonstrates proportionality to $|E_0|^6$, emphasizing the dominance of the three-photon absorption process in the excitation mechanism. However, as the field strength increases, the deviation from the three-photon absorption line indicates the initiation of a nonperturbative mechanism in the excitation process.

In contrast to the $|E_0|^6$-dependence of the number of photo-excited carriers in the weak field regime, the injected current and the corresponding population imbalance goes as $|E_0|^7$, as shown in Figure 7a. The difference in nonlinearities between the absolute photo-carrier population and the population imbalance suggests that the population imbalance is negligible concerning the absolute photo-carrier population in the weak field regime. However, in a strong field regime, the relative significance of the population imbalance may become substantial as it grows more rapidly than the absolute photocarrier population. Therefore, the distinction in nonlinearities between the total photocarrier population and the population imbalance indicates the potential for large-amplitude valley carrier population control.

To assess the population imbalance induced by a strong field in the deeply off-resonant regime, we calculate the population distribution $n_{c\vec{k}}$ after irradiating the laser field with a strength of 100 MVcm^{-1}. A clear pattern can be observed in the excited carrier population distribution around the K and K' points. This pattern may be understood through the multi-photon absorption resonances of the light-induced Floquet states.[32] In **Figure 8** a, the computed population distribution in the conduction band is shown. As anticipated from the preceding discussion, the photocarrier distribution reveals a significant population imbalance between $\boldsymbol{k}$ and $-\boldsymbol{k}$ points. To enhance clarity in visualizing the population imbalance, we compute the population imbalance distribution $\Delta n_{c\boldsymbol{k}} = n_{c\boldsymbol{k}} - n_{c,-\boldsymbol{k}}$. Figure 8b shows the resulting population imbalance distribution $\Delta n_{c\boldsymbol{k}}$. Since $\Delta n_{c\boldsymbol{k}}$ is constrained by $-1 \leq \Delta n_{c\boldsymbol{k}} \leq 1$, the population imbalance between $\boldsymbol{k}$ and $-\boldsymbol{k}$ is maximized when $|\Delta n_{c\boldsymbol{k}}| = 1$. As observed in Figure 8b, the population imbalance distribution takes significantly large values,

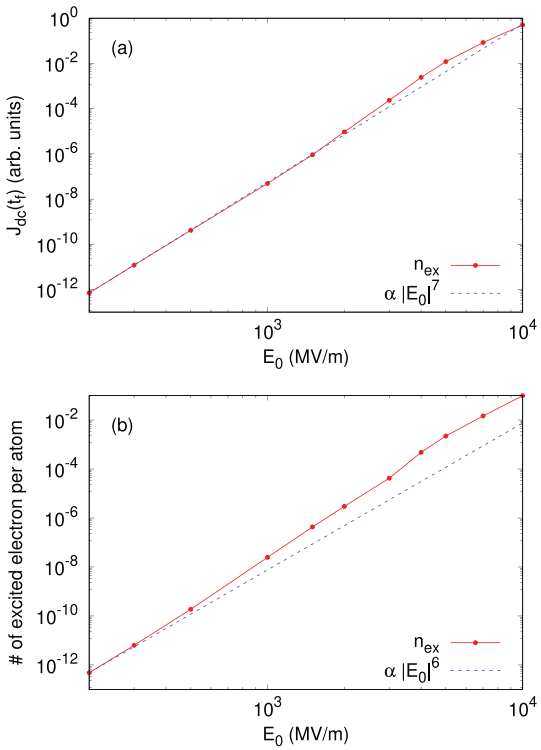

Figure 7. a) The persistent current, $|J_{dc}(t_f)|$, is shown as a function of the field strength, E_0. b) The number of conduction population after the laser irradiation is shown as a function of the field strength E_0.

comparable to the maximum values (±1), across a wide range of the Brillouin zone.

For further quantification, we calculate the population imbalance ratio r_{im} defined as

$$r_{im} = \frac{\int_{BZ} d\boldsymbol{k}|\Delta n_{ck}|}{\int_{BZ} d\boldsymbol{k}\left(n_{ck} + n_{c,-k}\right)} = \frac{\int_{BZ} d\boldsymbol{k}|\Delta n_{ck}|}{2\int_{BZ} d\boldsymbol{k} n_{ck}} \tag{10}$$

The computed imbalance ratio, r_{im}, from Figure 8 a,b is about 0.307. Hence, more than 30% of the excited electrons contribute to the population imbalance.

In the previous work,[16] significant control over valley population was proposed using bi-circular fields with counter-rotating ω and 2ω two-color laser fields. In this work, we demonstrate that significant valley population can be induced even without relying on circular or elliptically polarized light; rather, bi-color linearly polarized light alone can break time-reversal symmetry and cause such population control.

4. Summary

In this study, we conducted a theoretical exploration of light-induced electron dynamics in *h*-BN by solving the time-dependent Schrödinger equation, Equation (2), utilizing the tight-binding Hamiltonian defined in Equation (1). The driving force for electron dynamics was provided by two-color linearly-polarized laser fields, as expressed in Equation (5), with frequencies ω and 2ω.

Our initial investigation focused on analyzing the electric current induced by these two-color laser fields within the weak field regime. We confirmed that the dc-component of the induced current persists even after laser irradiation when the fundamental photon energy $\hbar\omega$ exceeds the optical gap, $E_g/2$. This ballistic current phenomenon originates from a population imbalance in the Brillouin zone, arising from quantum interference between two distinct excitation paths: one involving one-photon absorption at the photon energy of $2\hbar\omega$, and the other involving a two-photon absorption path at the photon energy of $\hbar\omega$.[17–19]

Expanding our analysis to the deeply off-resonant regime, where $\hbar\omega \ll E_g/2$, we observed an absence of population imbalance under weak applied field strength. However, as the field strength increased, a population imbalance in the Brillouin zone is formed, leading to the injection of the persistent dc-current after the laser irradiation. Scaling analysis of the ballistic current injection with respect to the applied field strength E_0 revealed that the population imbalance and the ballistic current result from an interference between three-photon absorption process with three photons of energy $2\hbar\omega$ and a four-photon absorption process with two photons of energy $2\hbar\omega$ and two photons of energy $\hbar\omega$. Consequently, we demonstrated that a multi-photon absorption process, incorporating photons with different energies, plays

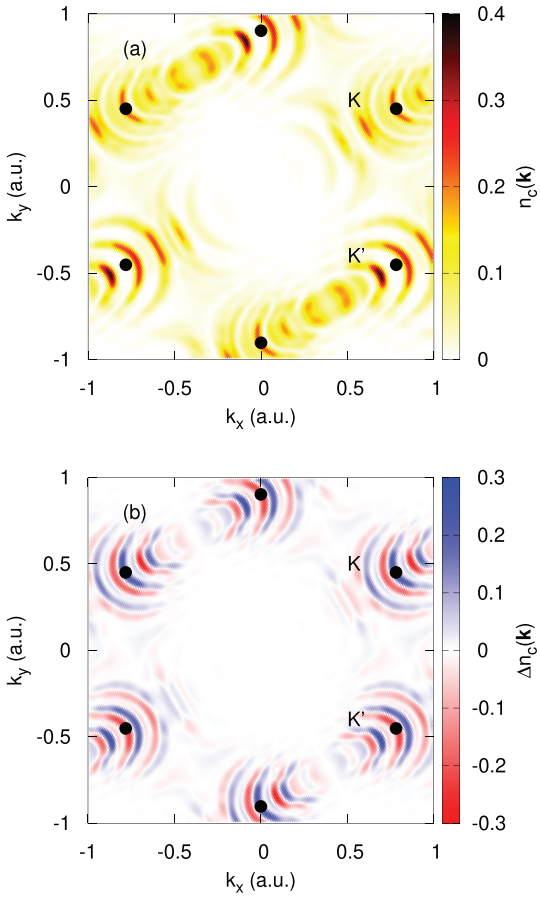

Figure 8. a) The conduction population distribution $n_c(\boldsymbol{k})$ after the irradiation of the laser field, and b) the population imbalance distribution $\Delta n_c(\boldsymbol{k})$ are shown. The results are computed by setting E_0 to 10^{10} Vm^{-1}.

a pivotal role in addition to the multi-photon absorption process involving single-color photons.

Our analysis of the population distribution of photo-excited electrons (Figure 8) indicated that more than 30% of excited electrons contribute to the population imbalance when the field strength E_0 reaches 100 MVcm^{-1}. This implies the potential for realizing a significant population imbalance through the use of linearly polarized light alone.

In previous works,[15,16] the formation of substantial population imbalance and valley-population control has been discussed in monolayer systems such as monolayer *h*-BN and graphene, using bi-circular laser fields with frequencies ω and 2ω. Recently, valley-population control with bi-circular fields has been extended to multi-layer and bulk systems[33] without relying on intrinsic inversion symmetry breaking and the Berry curvature at the valleys. In this work, our study demonstrates the induction of a large population imbalance and ballistic current injection even without relying on the ellipticity of light. Instead, we rely on time-reversal symmetry breaking achieved through relative phase control between two-color linearly-polarized fields at frequencies ω and 2ω. Furthermore, similar to Ref. [33], the injection mechanism with bi-color linearly polarized light does not rely on intrinsic inversion symmetry breaking, indicating an efficient dc current injection and population control with the scheme using linearly-polarized light. The potential of population control and the photovoltaic effect with linearly polarized light, in addition to circularly/elliptically polarized light, unveils novel avenues for realizing ultrafast opto-electronics, marked by precise control of current and population dynamics on the femtosecond time scale.

Acknowledgements

This work was supported by JSPS KAKENHI Grant Numbers JP20K14382 and JP21H01842, the Cluster of Excellence 'CUI: Advanced Imaging of Matter'- EXC 2056 - project ID 390715994, SFB-925 "Light induced dynamics and control of correlated quantum systems" — project 170620586 of the Deutsche Forschungsgemeinschaft (DFG), and the Max Planck-New York City Center for Non-Equilibrium Quantum Phenomena. The Flatiron Institute is a division of the Simons Foundation.

Open access funding enabled and organized by Projekt DEAL.

Conflict of Interest

The authors declare no conflict of interest.

Data Availability Statement

The data that support the findings of this study are available from the corresponding author upon reasonable request.

Keywords

nonlinear optics, photovoltaic effect

Received: March 8, 2024
Revised: June 4, 2024
Published online:

[1] J. E. Sipe, A. I. Shkrebtii, *Phys. Rev. B* **2000**, *61*, 5337.
[2] J. Seidel, D. Fu, S.-Y. Yang, E. Alarcón-Lladó, J. Wu, R. Ramesh, J. W. Ager, *Phys. Rev. Lett.* **2011**, *107*, 126805.
[3] T. Choi, S. Lee, Y. J. Choi, V. Kiryukhin, S.-W. Cheong, *Science* **2009**, *324*, 63.
[4] S. Y. Yang, J. Seidel, S. J. Byrnes, P. Shafer, C.-H. Yang, M. D. Rossell, P. Yu, Y.-H. Chu, J. F. Scott, J. W. Ager, L. W. Martin, R. Ramesh, *Nat. Nanotechnol.* **2010**, *5*, 143.
[5] Z. Dai, A. M. Rappe, *Chem Phys. Rev.* **2023**, *4*, 011303.
[6] N. Laman, A. I. Shkrebtii, J. E. Sipe, H. M. van Driel, *Appl. Phys. Lett.* **1999**, *75*, 2581.
[7] N. Laman, M. Bieler, H. M. van Driel, *J. Appl. Phys.* **2005**, *98*, 103507.
[8] A. Schiffrin, T. Paasch-Colberg, N. Karpowicz, V. Apalkov, D. Gerster, S. Mühlbrandt, M. Korbman, J. Reichert, M. Schultze, S. Holzner, J. V. Barth, R. Kienberger, R. Ernstorfer, V. S. Yakovlev, M. I. Stockman, F. Krausz, *Nature* **2013**, *493*, 70.
[9] G. Wachter, C. Lemell, J. Burgdörfer, S. A. Sato, X.-M. Tong, K. Yabana, *Phys. Rev. Lett.* **2014**, *113*, 087401.
[10] J. D. Lee, W. S. Yun, N. Park, *Phys. Rev. Lett.* **2016**, *116*, 057401.
[11] T. Higuchi, C. Heide, K. Ullmann, H. B. Weber, P. Hommelhoff, *Nature* **2017**, *550*, 224.
[12] C. Heide, T. Boolakee, T. Higuchi, P. Hommelhoff, *J. Phys.: Photon.* **2020**, *2*, 024004.
[13] Y. Morimoto, Y. Shinohara, K. L. Ishikawa, P. Hommelhoff, *New J. Phys.* **2022**, *24*, 033051.
[14] Á. Jiménez-Galán, R. E. F. Silva, O. Smirnova, M. Ivanov, *Nat. Photonics* **2020**, *14*, 728.
[15] M. S. Mrudul, Álvaro Jiménez-Galán, M. Ivanov, G. Dixit, *Optica* **2021**, *8*, 422.
[16] O. Neufeld, N. Tancogne-Dejean, U. De Giovannini, H. Hübener, A. Rubio, *Phys. Rev. Lett.* **2021**, *127*, 126601.
[17] E. Dupont, P. B. Corkum, H. C. Liu, M. Buchanan, Z. R. Wasilewski, *Phys. Rev. Lett.* **1995**, *74*, 3596.
[18] R. Atanasov, A. Haché, J. L. P. Hughes, H. M. van Driel, J. E. Sipe, *Phys. Rev. Lett.* **1996**, *76*, 1703.
[19] A. Haché, Y. Kostoulas, R. Atanasov, J. L. P. Hughes, J. E. Sipe, H. M. van Driel, *Phys. Rev. Lett.* **1997**, *78*, 306.
[20] D. Sun, C. Divin, J. Rioux, J. E. Sipe, C. Berger, W. A. de Heer, P. N. First, T. B. Norris, *Nano Lett.* **2010**, *10*, 1293.
[21] R. A. Muniz, C. Salazar, K. Wang, S. T. Cundiff, J. E. Sipe, *Phys. Rev. B* **2019**, *100*, 075202.
[22] C. Heide, T. Boolakee, T. Eckstein, P. Hommelhoff, *Nanophotonics* **2021**, *10*, 3701.
[23] K. Wang, R. A. Muniz, J. E. Sipe, S. T. Cundiff, *Phys. Rev. Lett.* **2019**, *123*, 067402.
[24] P. A. Roos, Q. Quraishi, S. T. Cundiff, R. D. R. Bhat, J. E. Sipe, *Opt. Express* **2003**, *11*, 2081.
[25] J. Sławińska, I. Zasada, Z. Klusek, *Phys. Rev. B* **2010**, *81*, 155433.
[26] X. Blase, A. Rubio, S. G. Louie, M. L. Cohen, *Phys. Rev. B* **1995**, *51*, 6868.
[27] D. R. Hofstadter, *Phys. Rev. B* **1976**, *14*, 2239.
[28] N. Nagaosa, J. Sinova, S. Onoda, A. H. MacDonald, N. P. Ong, *Rev. Mod. Phys.* **2010**, *82*, 1539.
[29] S. A. Sato, P. Tang, M. A. Sentef, U. D. Giovannini, H. Hübener, A. Rubio, *New J. Phys.* **2019**, *21*, 093005.
[30] S. A. Sato, A. Rubio, *Phys. Rev. B* **2024**, *109*, 195205.
[31] S. A. Sato, M. Lucchini, M. Volkov, F. Schlaepfer, L. Gallmann, U. Keller, A. Rubio, *Phys. Rev. B* **2018**, *98*, 035202.
[32] A. Galler, A. Rubio, O. Neufeld, *J. Phys. Chem. Lett.* **2023**, *14*, 11298.
[33] I. Tyulnev, Á. Jiménez-Galán, J. Poborska, L. Vamos, R. F. Silva, P. S. J. Russell, F. Tani, O. Smirnova, M. Ivanov, J. Biegert, Valleytronics in bulk mos_2 by optical control of parity and time symmetries, **2023**, arXiv:2302.12564 [cond-mat.mtrl-sci].